Applied Surface Science 390 (2016) 368–376

Contents lists available at ScienceDirect

Applied Surface Science

journal homepage: www.elsevier.com/locate/apsusc

Synthesis of surface molecular imprinted TiO_2/graphene photocatalyst and its highly efficient photocatalytic degradation of target pollutant under visible light irradiation

Cui Lai[a,b,*], Man-Man Wang[a,b], Guang-Ming Zeng[a,b,*], Yun-Guo Liu[a,b], Dan-Lian Huang[a,b], Chen Zhang[a,b], Rong-Zhong Wang[a,b], Piao Xu[a,b], Min Cheng[a,b], Chao Huang[a,b], Hai-Peng Wu[a,b], Lei Qin[a,b]

[a] College of Environmental Science and Engineering, Hunan University, Changsha 410082, Hunan, PR China
[b] Key Laboratory of Environmental Biology and Pollution Control (Hunan University), Ministry of Education, Changsha 410082, Hunan, PR China

ARTICLE INFO

Article history:
Received 28 June 2016
Received in revised form 10 August 2016
Accepted 22 August 2016
Available online 24 August 2016

Keywords:
TiO_2/graphene
Surface molecular imprinting technique
Molecular recognition
Photocatalytic activity
Bisphenol A

ABSTRACT

The molecular imprinted TiO_2/graphene photocatalyst (MIP-TiO_2/GR) was successfully prepared with bisphenol A (BPA) as the template molecule (target pollutant) and o-phenylenediamine (OPDA) as functional monomers by the surface molecular imprinting method. The combination between BPA and OPDA led to the formation of the precursor, and the subsequent polymerization of OPDA initiated by ultraviolet radiation can ensure the realization of MIP-TiO_2/GR. The samples were characterized by SEM, EDS, XRD, BET, UV–vis DRS and Zeta potential. In addition, adsorption capacities, adsorption selectivity and visible light photocatalytic performances of MIP-TiO_2/GR and non-imprinted TiO_2/graphene (NIP-TiO_2/GR) were evaluated. Moreover, the effects of pH and initial BPA concentration on removal efficiency of BPA were also investigated. The results showed that MIP-TiO_2/GR exhibited better adsorption capacity and adsorption selectivity towards the template molecule compared to NIP-TiO_2/GR due to the imprinted cavities on the surface of MIP-TiO_2/GR. Moreover, the photocatalytic activity of MIP-TiO_2/GR toward the target molecules was stronger than that of NIP-TiO_2/GR as a result of large adsorption capacity to target molecules and narrow band gap energy on MIP-TiO_2/GR. Therefore, modifying the photocatalyst by the surface molecular imprinting is a promising method to improve the molecule recognition and photocatalytic efficiency of photocatalyst for target pollutant.

1. Introduction

Nowadays, with the development of the industrialization and the abuse of plastics, contamination of endocrine disrupter has been widely caused [1,2], and has become a widespread concerned environmental problem in the world along with greenhouse effect and ozone depletion in most cases [3,4]. Bisphenol A (4,4-Isopropylidenediphenol, BPA) is one of the endocrine disrupter, and removing BPA from circumstance is urgent due to its tendency to bio-accumulate, even at very low concentrations, which will disturb human health through affecting endogenous hormones. It is commonly known that semiconductor photocatalytic process has been regarded as an effective treatment approach for the removal of organic pollutants in wastewater [5], because it is not influenced by their toxicity and the process will not produce new pollutants. Currently, there is a strong focus on TiO_2 in the semiconductor photocatalyst field [6,7], since it is low environmental impact, high stable, strong oxidization power, and low-priced [8]. When the kind of catalytic material TiO_2 is irradiated by light reaching or exceeding its band gap energy, electron-holes are formed and they separately react to O_2 and H_2O or OH^- producing hydroxyl radicals (•OH) with high oxidability which get rid of pollutants [9]. However, the disadvantages such as a large bandgap, harmful recombination of photogenerated electron-holes, low affinity and poor selection for contaminant, result in a poor performance of TiO_2 in photoactivity in the visible light [10,11]. Thus, it is expected to enhance the utilization rate of light and selective recognition performance of TiO_2 to remove the target pollutants under visible light.

For improving the photocatalytic performance of TiO_2, the currently conventional technologies including doped with metal ion [10,12] or nonmetallic elements [13,14], coupled with the semicon-

* Corresponding authors at: College of Environmental Science and Engineering, Hunan University, Changsha 410082, Hunan, PR China.
E-mail addresses: laicui@hnu.edu.cn (C. Lai), zgming@hnu.edu.cn (G.-M. Zeng).

http://dx.doi.org/10.1016/j.apsusc.2016.08.119
0169-4332/

ductor [15–17] and fixed in the large surface area of the material such as mesoporous material [18], zeolite [19,20] or carbon based materials and so on [21,22]. Graphene, an sp_2-bonded carbon sheet, has attracted much attentions because of its tunable surface properties including large surface area used for the supporter of nanosized particles, the high electronic conductivity worked for facilitating charge transportation and separation, and the hydroxyl groups located on edges served for the hydrophilia and favorable reactive sites for guest materials [23–25]. On the one hand, the addition of graphene into TiO_2 suppresses the recombination of photogenerated electron-hole. Moreover, the carbon of nonmetallic element co-doped titania enhances broad light absorption [26]. Hence, the photocatalytic performance of composite material with TiO_2 will be enhanced.

In recent years, coating TiO_2 with an organic layer of molecularly imprinted polymers (MIP) is also applied to enhance the photocatalytic degradation efficiency through improving the ability of recognition and the adsorption quantity for the aimed pollutants [27–29]. MIPs can recognize the template molecule through its highly selective synthetic polymer receptors. Traditionally, MIPs are synthesized by the copolymerization of functional monomer and cross-linkers assembled around the target molecules (template) in an aprotic and nonpolar solvent [30]. In our work, o-phenylenediamine (OPDA) was chosen as the functional monomer. Its two $-NH_2$ groups are not only hydrophilic to enhance the hydrophilia but also can interact with functional group (—OH) of the target molecules (BPA) to form a precursor, ensuring the imprinting of the templates molecules during polymerization [29]. Besides, the polymer with a polyaniline-like structure produced with the aid of UV light illumination of OPDA has the good chemical and photochemical stability. In addition, the excess OPDA failed to form a precursor with the template molecules may function as cross-linker [31]. Therefore, OPDA is selected to realize the combination of molecular imprinting and titanium dioxide for selective recognition of template molecules in wastewater.

The intent of the present work was to investigate the specific recognition and catalytic effect of composite photocatalyst as a plausible technique for the treatment of BPA in wastewater. The adsorption capacities and adsorptive selectivity of molecular imprinted TiO_2/graphene (MIP-TiO_2/GR) and non-imprinted TiO_2/graphene (NIP-TiO_2/GR) was tested in dark, respectively. Phenol was used as the probe molecule to test the adsorptive selectivity of MIP-TiO_2/GR, since phenol had similar functional group to BPA. The photocatalytic activities were evaluated in water under visible-light irradiation and the effects of pH and initial BPA concentration on removal efficiency of BPA were also investigated. The photocatalyst of MIP-TiO_2/GR was compared with NIP-TiO_2/GR from morphology, structure, adsorption capacity, adsorptive selectivity and photocatalytic activity in this work.

2. Experimental

2.1. Materials

Tetrabutyl orthotitanate ($Ti(OBu)_4$) and o-phenylenediamine (OPDA) were purchased from Sinopharm Chemical Reagent Co.,Ltd. (China). Graphite powder (99 wt%), $KMnO_4$ (98 wt%), H_2SO_4 (98 wt%), H_2O_2 (30 wt%) and ethanol were purchased from Sinopharm Chemical Reagent Co.,Ltd. (China). BPA (purity > 99%) were supplied from Tianjin Guangfu Fine Chemical Research Institute. All the chemicals were of analytical reagent grade and used as received without further purification. The water used is ultrapure water (18.2 MΩ Cm, Milli-Q Millipore) in experimental process. HPLC-grade acetonitrile was purchased from Tedia Company Inc. (USA).

2.2. Preparation of surface molecular imprinted TiO_2/graphene photocatalyst

2.2.1. Preparation of TiO_2/grapheme photocatalyst

Firstly, TiO_2/graphene (TiO_2/GR) photocatalyst was synthesized according to a facile solvothermal synthesis method. The process followed the reference of Yang et al. [23]. Briefly, 40 mg of the graphene oxide (GO) synthesized by modified Hummers' method was dispersed in 140 mL of glacial acetic acid in an erlenmeyer flask [32]. The flask was sealed and sonicated for 3 h, and then tetrabutyl titanate (TBT, 4 mL) was dropwise added into the above GO suspension under magnetic stirring. The mixture was stirred for 10 min and then transferred into a 200 mL teflon-lined stainless steel autoclave heated at 180 °C for 24 h. The obtained precipitate was collected by centrifugation, washed several times with absolute ethanol, and dried at 60 °C in vacuum overnight. The mass ratio of graphene and TiO_2 in TiO_2/graphene is 1:23.

2.2.2. Preparation of MIP-coated TiO_2/graphene photocatalyst

MIP-coated TiO_2/graphene photocatalyst was modified to that described in previous work [28,29]. Typically, 0.107 g BPA and 0.24 g OPDA were dissolved in 20 mL of ethanol. Then 20 mL ultrapure water was added to the above solution and stirred for 20 min under magnetic stirring. The pH value of the solution was adjusted to 2.0 and 0.4 g of TiO_2/GR photocatalyst was further added. Then the mixture was sonicated for 3 min, followed by initiating with UV irradiation (165 W Hg lamp) for 1 h. After a polymerization reaction for 24 h, the templates were removed by Na_2CO_3 solution (0.2 g/L) for 5 times. Subsequently, the product was washed with distilled water to remove residual Na_2CO_3 solution and dried at 60 °C in vacuum overnight. The product was signed as MIP-TiO_2/GR. When no template (BPA) was used in the preparation, the obtained product was referred to as NIP- TiO_2/GR.

2.3. Characterization

The morphologies of the resulting samples were characterized by an environmental scanning electron microscope (SEM) (FEI QuANTA 200, Czekh). Energy dispersive spectrometry (EDS, Czekh) analysis was used to confirm the existence of OPDA in MIP-TiO_2/GR and NIP-TiO_2/GR composites. The X-ray diffraction (XRD) patterns were carried out with D5000 diffractometer operating with Cu-Kα source to investigate the crystal structure of the samples. UV-3310 scan UV–vis diffuse-reflectance spectra of as-synthesized samples were recorded in the range of 200–800 nm, using $BaSO_4$ as a reflectance reference. The Brunauer–Emmett–Teller (BET) surface area of MIP-TiO_2/GR and NIP-TiO_2/GR were measured with an automatic instrument (ASAP2020 M + C, Micromeritics, USA). Zeta potential of MIP-TiO_2/GR or NIP-TiO_2/GR was measured using a Zeta potential analyzer (Malvern Nano ZS90).

2.4. Adsorption performance in the dark

2.4.1. Adsorption kinetics in dark

150 mg TiO_2/GR, MIP-TiO_2/GR or NIP-TiO_2/GR was placed in a 200 mL conical flask and mixed with 150 mL of 8 mg/L BPA solution. The samples were oscillated in the absence of light at 25 °C. Samples were then taken out at regular time intervals, centrifuged at 12,000 rpm for 8 min and filtered using a membrane filter (0.22 μm). The concentration of free BPA in the solution was measured by high performance liquid chromatography (HPLC) at 226 nm. The concentration of BPA was calculated by a calibration curve.

2.4.2. Adsorption isotherm in the dark

20 mg TiO_2/GR, MIP-TiO_2/GR or NIP-TiO_2/GR was mixed with 20 mL BPA solution with initial concentrations ranging from 2 to 90 mg/L. After stirred for 2 h in dark, the solution was filtered and the remained supernatant concentration of BPA was measure by HPLC. The adsorption capacity (Q) was calculated as follows:

$$Q = (C_0 - C_e)V/W \quad (1)$$

where C_0 (mg/L) and C_e (mg/L) are the initial and adsorption equalized BPA solution concentrations, respectively. V (mL) is the sample volume, and W (g) is the mass of the catalysts.

2.5. Competitive batch rebinding tests in dark

In the competitive batch rebinding tests, the selectivity of MIP-TiO_2/GR and NIP-TiO_2/GR was measured in dark. 20 mg of MIP-TiO_2/GR or NIP-TiO_2/GR were added into 50 mL flasks, each of which contained 20 mL solution with initial concentrations of 8 mg/L of phenol and BPA in single and binary solutions. The adsorption mixture was oscillated in dark for 2 h and analyzed concentrations by HPLC at 226 nm for phenol and BPA. The recognition selectivity was measured by the static distribution coefficient (K_D) and selectivity coefficient (α). K_D and α were defined as follows [33]:

$$K_D = C_p/C_s \quad (2)$$

where C_p is the amount of ligand adsorbed and Cs is the concentration of free ligand.

$$\alpha = K_{D1}/K_{D2} \quad (3)$$

where K_{D1} and K_{D2} are the static distribution coefficients of template and competitive molecules.

2.6. Measurements of photocatalytic activity

The photocatalytic activities of MIP-TiO_2/GR and NIP-TiO_2/GR were evaluated by monitoring the photodegradation of BPA solution. A 300 W xenon lamp (CEL-HXE300, Beijing China Education Au-light Co., Ltd.) was used as a visible light resource with a 400 nm cutoff filter. For a typical experimental process, 150 mg MIP-TiO_2/GR and NIP-TiO_2/GR photocatalysts (1.0 g/L) was added into 150 mL of BPA solution and stirred in dark for 40 min to achieve the adsorption equilibrium and the equilibrium concentration of BPA was determined as the initial concentration C_0. Under continuous stirring, then irradiation started and samples were taken out at regular time intervals (20 min). The suspension solution was centrifuged at 12000 rpm for 8 min and filtered through a 0.22 μm filter. The BPA supernatant concentrations (C) at various time was measured by HPLC. The effect of initial pH and initial BPA concentration on the photocatalytic activity of MIP-TiO_2/GR was also studied. The solution pH was adjusted to successive initial values between 3.0 and 10.0 using HNO_3 or NaOH solution. The initial BPA concentration was adjusted to 4 mg/L, 8 mg/L, 16 mg/L, 24 mg/L and 32 mg/L, respectively.

2.7. Apparatus and methods

The detection of BPA was performed by HPLC (Agilent Technologies 1200 series) equipped with a C18 column and UV detector (DAD). The mobile phase was acetonitrile/water (45/55, v/v) at a flow rate of 1 mL/min and the column temperature was 35 °C and the injection volume was 20 μL. The detection wavelengths were selected at 226 nm. The standard curve for BPA is linearly best fitted (R^2 = 0.9998) with the concentration of BPA varied from 1 to 50 mg/L.

3. Results and discussion

3.1. Principle of preparation of MIP-TiO_2/GR photocatalyst

MIP-TiO_2/GR photocatalyst was synthesized by molecular imprinting technique and was shown in Fig. 1. Firstly, TiO_2/GR was produced via solvothermal synthesis method. During this process, the graphene oxide was reduced to graphene under high temperature and high pressure [23]. Then, the two amino groups (—NH_2) in o-phenylenediamine (OPDA) were able to interact with hydroxyl group (-OH) of the template molecule, leading to the formation of the precursor. The precursor between the functional monomer of OPDA and the template molecule of BPA was formed attributing to the hydrogen-bonding or electrostatic interactions, which was necessary for MIP coating [29]. Meanwhile, the monomer OPDA can also be adsorbed on the surface of the TiO_2 particles so that the polymer can be coated the surface of TiO_2/GR via polymerization initiated by ultraviolet radiation. During polymerization, the OPDA monomers produced a polymer (poly-o-phenylenediamine) with a polyaniline-like structure, which is favorable to the separation of photo-generated electron hole pairs to enhance the photocatalytic efficiency. Moreover, the excess OPDA molecules may serve as cross-linker, increasing the stable selectivity of the MIP layer. Finally, the template molecules in molecularly imprinted photocatalyst were washed with Na_2CO_3 solution and water.

3.2. Structural characterization

The morphology of the as-prepared photocatalysts of TiO_2/GR, NIP-TiO_2/GR and MIP-TiO_2/GR was investigated by the SEM in Fig. 2(a–c), respectively. The size of the TiO_2/GR particles ranged from 250 to 350 nm, and the particles tended to agglomerate. The morphology of the NIP-TiO_2/GR and MIP-TiO_2/GR particles is similar to each other. Some of the big flocculent particles can be seen from Fig. 2(a) and they decrease at Fig. 2(b and c). The big flocculent particles may be the precipitations of titanium compounds which are not chemical reaction completely. The decrease of particles may be the result of many times of washing following a subsequent experiment process of NIP-TiO_2/GR and MIP-TiO_2/GR. Meanwhile, combined with the BET analysis that the specific surface areas of NIP-TiO_2/GR and MIP-TiO_2/GR are 122 m^2/g and 124 m^2/g, the results are consistent with SEM images. The deposited coatings on the surface of TiO_2/GR particles may be too thin, so that the specific surface area of MIP-TiO_2/GR is a little larger than that of NIP-TiO_2/GR. The contribution of the imprinted cavities is very small in increasing the specific surface area [33].

EDS analysis is employed to prove that OPDA exists in NIP-TiO_2/GR and MIP-TiO_2/GR photocatalysts. In our cases, Fig. 2(d and e) showed that the weight percent of nitrogen was 10.59 and 11.51 in NIP-TiO_2/GR and MIP-TiO_2/GR respectively, showing the existence of poly-o-phenylenediamine. Meanwhile, the preparation process of NIP-TiO_2/GR and MIP-TiO_2/GR was similar excepting the NIP-TiO_2/GR without the template molecule, so that results of element analysis of NIP-TiO_2/GR and MIP-TiO_2/GR are not quite different. The EDS analysis results conformed to the SEM images.

It has been reported that anatase TiO_2 exhibits high photocatalytic activity in the photodegradation of most pollutants [34]. The X-ray diffraction (XRD) patterns of TiO_2/GR, NIP-TiO_2/GR and MIP-TiO_2/GR are shown in Fig. 3. The results of XRD data show that the major phase of the photocatalyst is anatase phase and match well with the standard anatase pattern (PDF#21-1272) [23]. In addition, the rutile phase was not significant observed. The characteristic peaks at 2θ of 25.3°, 37.8°, 48.0°, 53.9°, 55.1°, and 62.7° represent the indices of (101), (004), (200), (105), (211), and (204) reflection of anatase TiO_2, respectively. The diffraction peak for GR is visible at 2θ of 26.6° [7] and the diffraction peak for poly-o-phenylenediamine

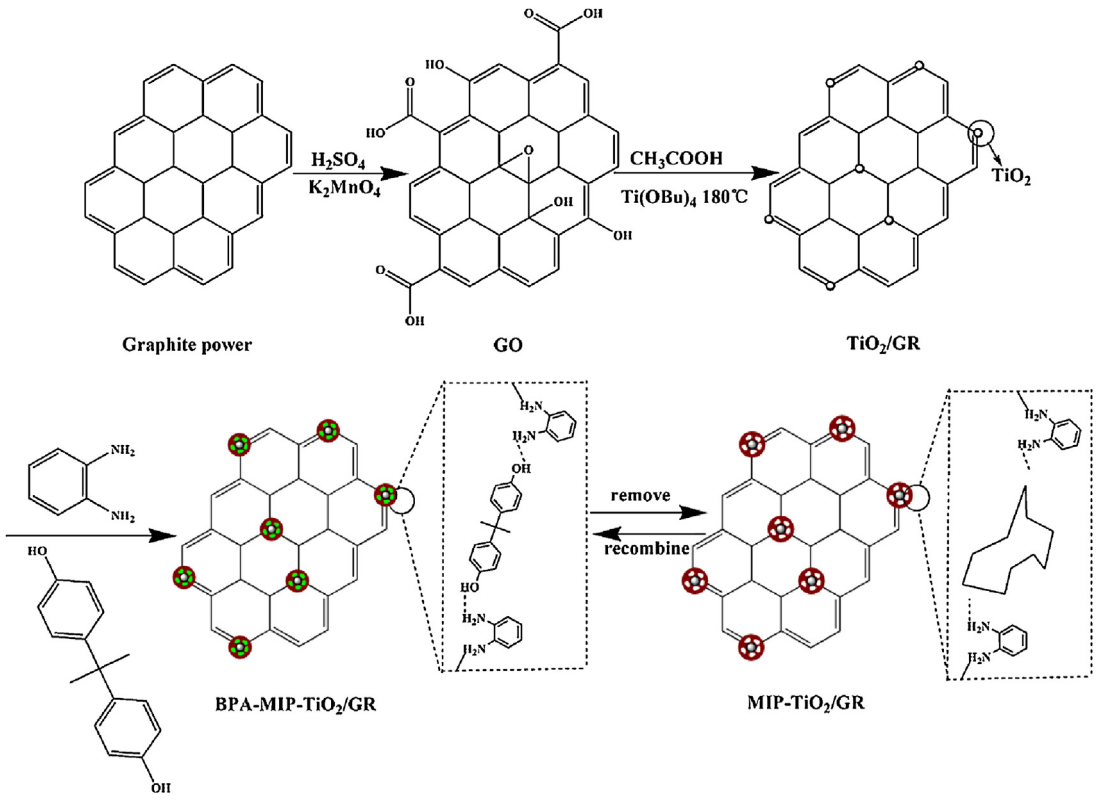

Fig. 1. Schematic illustration of the preparation processes of molecular imprinted TiO_2/graphene (MIP-TiO_2/GR).

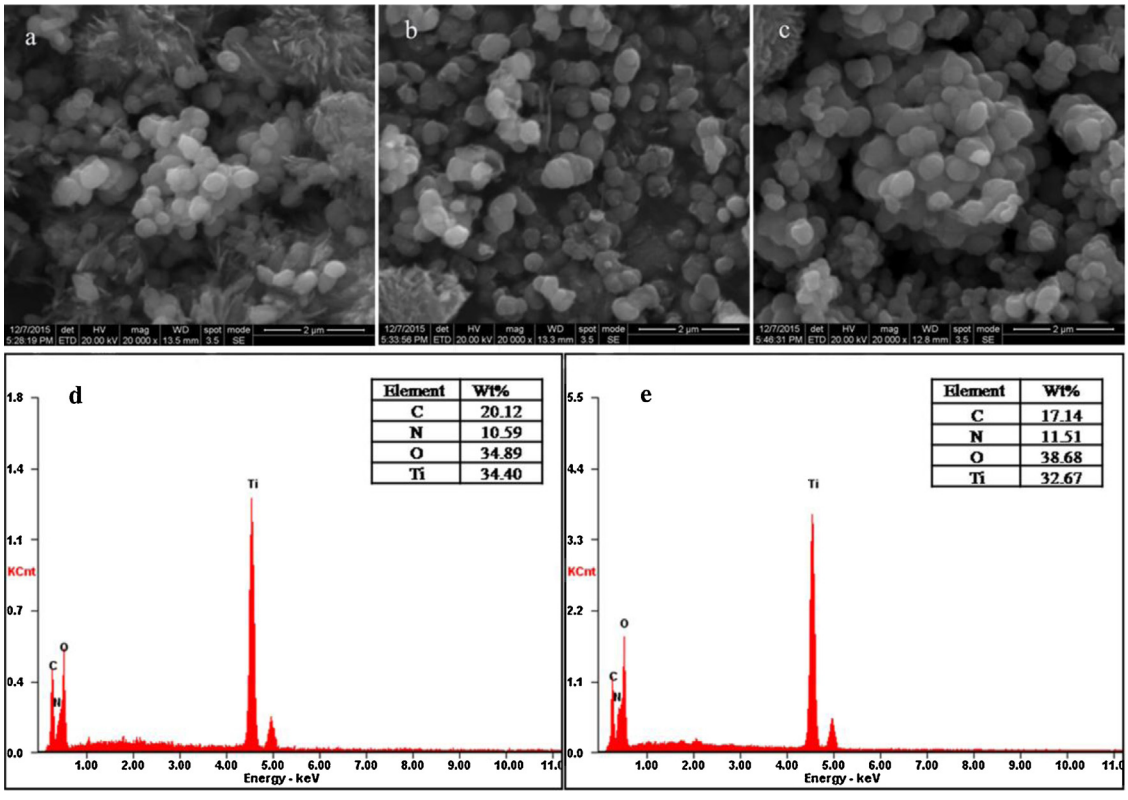

Fig. 2. SEM images of TiO_2/GR (a), NIP-TiO_2/GR (b) and MIP-TiO_2/GR (c) and EDS image of NIP-TiO_2/GR (d) and MIP-TiO_2/GR (e).

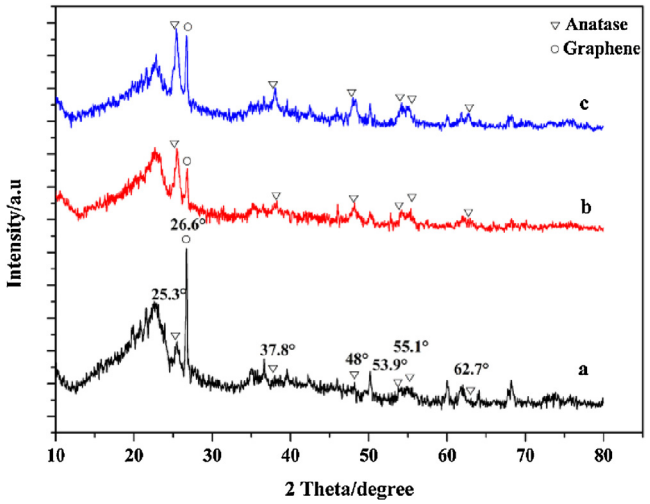

Fig. 3. XRD patterns of TiO_2/GR (a), NIP-TiO_2/GR (b) and MIP-TiO_2/GR (c).

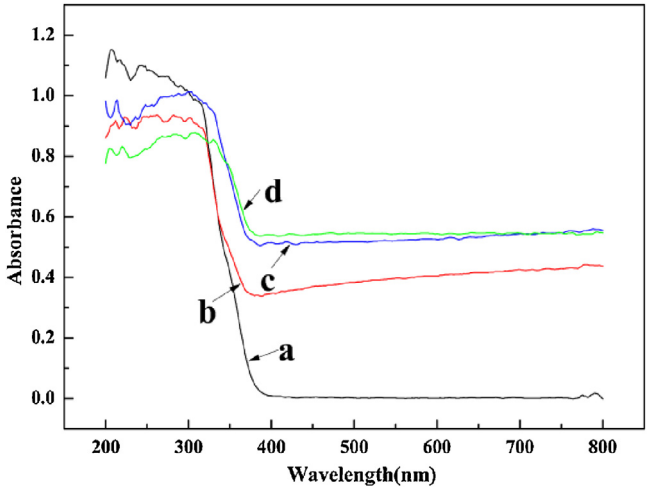

Fig. 4. UV–vis diffuse reflectance spectra of TiO_2 (a), TiO_2/GR (b), NIP-TiO_2/GR (c) and MIP-TiO_2/GR (d).

is invisible because it exists on the surface of TiO_2 [35], failed to change the crystalline structure of TiO_2.

UV–vis diffuse reflectance spectra of TiO_2, TiO_2/GO, NIP-TiO_2/GR and MIP-TiO_2/GR particles are shown in Fig. 4. Compared with pure TiO_2, TiO_2/GR exhibits stronger light absorption in visible region as a result of the graphene introduction. Compared with TiO_2/GR, the absorption boundary of NIP-TiO_2/GR and MIP-TiO_2/GR obviously shifts to higher wavelength and the absorption intensity is further enhanced in visible region. Furthermore, the absorption edge MIP-TiO_2/GR is higher than that of NIP-TiO_2/GR. The red shift of NIP-TiO_2/GR and MIP-TiO_2/GR photocatalyst indicates that the organic polymer with a polyaniline-like structure produced via the polymerization of OPDA under UV irradiation can effectively enhance the absorbency of light. In addition, the red shift of absorption edge means the decrease of the band gap of the photocatalyst. The lower band gap energy can be excited to produce more electron-hole pairs under visible light, which result in stronger photocatalytic activities, and the higher light-absorption intensity usually means better photocatalytic performance [11,33]. So, MIP-TiO_2/GR possesses higher photocatalytic activity than NIP-TiO_2/GR.

Zeta potential of MIP-TiO_2/GR and NIP-TiO_2/GR is shown in Fig. 5. A physical parameter of zeta potential can be used to quantify the electrical potential of the solid particle surface. The surface charge density changes with the increase of pH value and the pH_{zpc} of MIP-TiO_2/GR and NIP-TiO_2/GR is 7.55 and 3.55, respectively. The pH_{zpc} of MIP-TiO_2/GR shifts to higher values than that of NIP-TiO_2/GR and the results suggest that more positive sites are available on the surface of MIP-TiO_2/GR in the pH range studied. Similarly, the pH_{zpc} of MIP-TiO_2/SiO_2 was be found to be higher than that of NIP-TiO_2/SiO_2 [34]. When the pH value is lower than pH_{zpc}, the surface charge was positive. Meanwhile, when the pH value is higher than pH_{zpc}, the surface charge was negative. The positive charge has higher affinity for anions and the negative charge has higher affinity for cations. Besides, the zeta potentials of MIP-TiO_2/GR and NIP-TiO_2/GR are significantly different at pH 6.0. Hence, the surface charge may be one of the reasons for the different adsorption capacities of MIP-TiO_2/GR and NIP-TiO_2/GR for BPA.

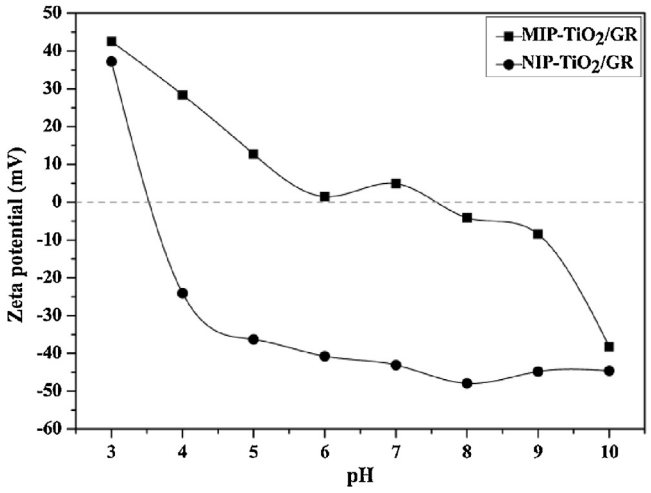

Fig. 5. Zeta potential of MIP-TiO_2/GR and NIP-TiO_2/GR samples suspended in 20 mL BPA solution as a function of pH.

3.3. The adsorption properties of TiO_2/GR, MIP-TiO_2/GR and NIP-TiO_2/GR in the dark

3.3.1. Adsorption kinetics of the TiO_2/GR, MIP-TiO_2/GR and NIP-TiO_2/GR

Adsorption kinetics, one of the most important characters of adsorption efficiency, can influence subsequent photocatalytic reaction. The adsorption kinetics is investigated with 8 mg/L BPA solution, a pH of 6.0 and the photocatalyst concentration of 1 g/L. Fig. 6(a) shows the dynamic curves for the adsorption of BPA on TiO_2/GR, NIP-TiO_2/GR and MIP-TiO_2/GR. It can be seen that the adsorption amounts of BPA on TiO_2/GR, NIP-TiO_2/GR and MIP-TiO_2/GR increase rapidly within 5 min, and then adsorption equilibrium is gradually established within 10 min. The adsorption amount has no obvious change from 10 to 40 min. In addition, the adsorption amount of TiO_2/GR is close to the NIP-TiO_2/GR and the adsorption amount of MIP-TiO_2/GR is higher than that of NIP-TiO_2/GR and TiO_2/GR. The enhanced adsorption capacity of MIP-TiO_2/GR may be taking advantage of the increasing adsorption sites and good affinity of imprinted cavities [34].

3.3.2. Adsorption isotherm of the TiO_2/GR, MIP-TiO_2/GR and NIP-TiO_2/GR

Fig. 6(b) exhibits the adsorption isotherms of TiO_2/GR, MIP-TiO_2/GR and NIP-TiO_2/GR over BPA in dark. The adsorption isotherms is investigated with a pH of 6.0. From Fig. 6(b), we can see that the adsorption capacity (Qe) increases rapidly with

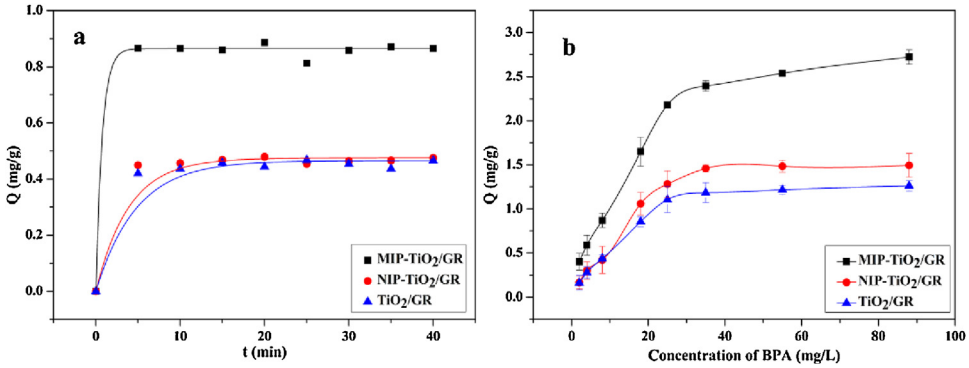

Fig. 6. Kinetics of adsorption (a) and adsorption isotherm (b) for bisphenol A (BPA) over TiO_2/GR, MIP-TiO_2/GR and NIP-TiO_2/GR.

the increase of the concentration of BPA in the range of the concentration of 2 mg/L–25 mg/L, while it increases slightly and finally reaches saturated adsorption in the range of the concentration of 25 mg/L–90 mg/L. Meanwhile, the saturated adsorption capacity of NIP-TiO_2/GR is higher than that of TiO_2/GR because of the polymer coated the surface of TiO_2/GR. Furthermore, the adsorption capacity of MIP-TiO_2/GR is consistently higher than that of TiO_2/GR and NIP-TiO_2/GR attributing to the imprinted cavities on the surface of MIP-TiO_2/GR in this process. Hence, the MIP-TiO_2/GR is expected to show higher photocatalytic degradation ability to the template molecules of BPA in comparison with NIP-TiO_2/GR [33]. The inference will be proved in the following experiment.

3.4. Adsorption selectivity test

In order to test the adsorption selectivity of MIP-TiO_2/GR and NIP-TiO_2/GR towards BPA in single and binary solution system, phenol is chosen as a competitor of BPA because of its common functional groups of hydroxyl groups with BPA. The results in single (a) and dual (b) solutions are shown in Fig. 7. From Fig. 7(a), it can be observed that the adsorption capacity of MIP-TiO_2/GR for phenol and BPA is larger than that of NIP-TiO_2/GR. Meanwhile, the adsorption capacity of MIP-TiO_2/GR is greater for BPA than that for phenol. The results indicate that MIP-TiO_2/GR and NIP-TiO_2/GR have adsorption capacity for phenol and BPA, and MIP-TiO_2/GR exhibits larger selectivity between phenol and BPA than NIP-TiO_2/GR due to the imprinted cavities on the surface of MIP-TiO_2/GR. In dual system (b) solutions, the selectivity of MIP-TiO_2/GR between phenol and BPA is also higher than that of NIP-TiO_2/GR. In order to intuitively understand the selectivity of MIP-TiO_2/GR and NIP-TiO_2/GR, the C_p, C_s, K_D and α are given in Table 1. The adsorption capacities of MIP-TiO_2/GR for BPA and phenol are higher than those of NIP-TiO_2/GR by the static distribution coefficient of K_D. Moreover, compared with phenol, MIP-TiO_2/GR is easier to combine with BPA according to the distribution coefficient α. Two results above indicate that the selectivity of MIP-TiO_2/GR between BPA and phenol is still obvious and imprinted cavities play an important role.

3.5. Degradation ability of MIP-TiO_2/GR

3.5.1. Degradation kinetics of BPA on MIP-TiO_2/GR and NIP-TiO_2/GR under visible light irradiation

The photocatalytic abilities of MIP-TiO_2/GR and NIP-TiO_2/GR photocatalysts are estimated on the basis of the kinetic data for the degradation of BPA under visible light irradiation with a pH of 6.0, BPA concentration of 8.0 mg/L and a catalyst concentration of 1.0 g/L. The result is shown in Fig. 8. The curve is fitted the first kinetic and the second kinetic line to investigate the kinetic behavior of photo-degradation BPA over MIP-TiO_2/GR and NIP-TiO_2/GR. The outside line is the first kinetic curve and the inset line is the second kinetic curve. The first kinetic equation is described using the following equation:

$$\ln\left(C_0/C\right) = kt \tag{4}$$

where C is the concentration of BPA (mg/L) at time t (min), C_0 is the concentration of BPA (mg/L) at t = 0 (min), and k is the reaction rate constant (min^{-1}). The rate constant k can be determined from the slope of linear plot. The second kinetic equation is described using the following equation:

$$1/C = kt + b \tag{5}$$

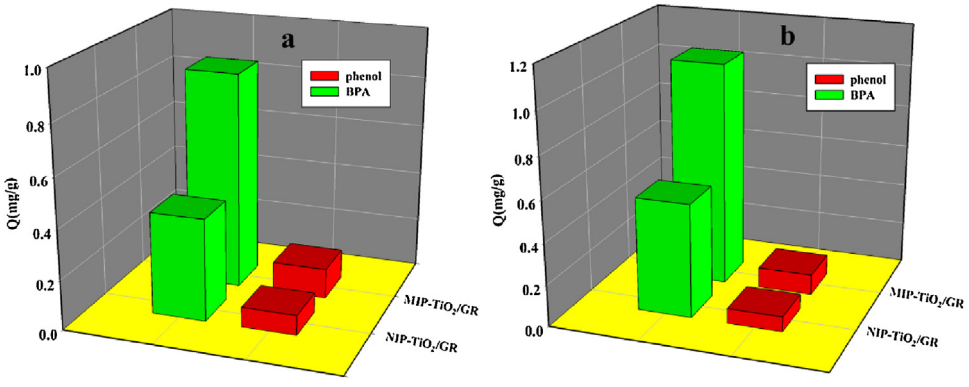

Fig. 7. Adsorption capacity of MIP-TiO_2/GR and NIP-TiO_2/GR in single adsorbate (a) and dual adsorbate (b) solutions.

Table 1
Distribution and selectivity coefficient of bisphenol A (BPA) in the dual system for MIP-TiO_2/GR and NIP-TiO_2/GR.

adsorbate	C_p		C_s		K_D		α	
	MIP	NIP	MIP	NIP	MIP	NIP	MIP	NIP
phenol	0.0985	0.0722	7.9015	7.9278	0.0125	0.0091	12.3920	8.0549
BPA	1.0732	0.5462	6.9286	7.4538	0.1549	0.0733		

[a] C_p is the amount of ligand adsorbed and C_s is the free ligand concentration.
[b] K_{D1} and K_{D2} are the static distribution coefficients of template and competitive molecules.

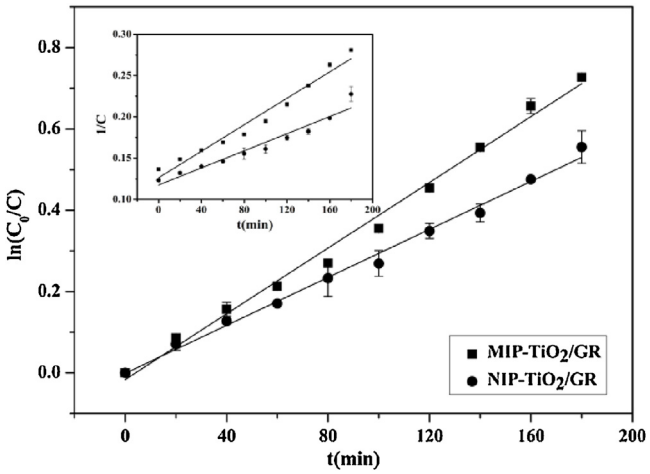

Fig. 8. The first kinetic (outside) and the second kinetic (inset) of photocatalytic degradation bisphenol A (BPA) over MIP-TiO_2/GR and NIP-TiO_2/GR.

Table 2
Kinetics parameters for photocatalytic degradation bisphenol A (BPA).

Photocatalyst	First kinetic equation		Second kinetic equation	
	k_1	R^2	k_2	R^2
MIP-TiO_2/GR	0.00404	0.99047	0.00080	0.96485
NIP-TiO_2/GR	0.00295	0.99234	0.00052	0.93908

[a] k_1 is the rate constant of first kinetic photocatalytic degradation and k_2 is the rate constant of second kinetic photocatalytic degradation.
[b] R^2 is the correlation coefficient.

Kinetics parameters for photocatalytic degradation BPA over MIP-TiO_2/GR and NIP-TiO_2/GR are listed in Table 2. From the results, it can be found that the rate constant k of MIP-TiO_2/GR composites are both higher than that of NIP-TiO_2/GR in the first kinetic equation and the second kinetic equation. It shows that the photocatalytic activity of MIP-TiO_2/GR is superior to NIP-TiO_2/GR. Meanwhile, the first kinetic linear regression coefficients (R^2) are higher than the second kinetic linear regression coefficients. It indicates that the first kinetic equation is better match the process of degradation. All these show that the imprinted cavities on the surface of MIP-TiO_2/GR may be the significant effect on the enhancement of photocatalytic activity. The high photocatalytic efficiency of MIP-TiO_2/GR is attributed to the narrow band gap energy, high light-absorption intensity in visible light regions and large adsorption capacity of MIP-TiO_2/GR for BPA [11,34]. Hence, it is proved that MIP-TiO_2/GR has promising perspective under visible light activity.

3.5.2. *Effects of pH on degradation of BPA on MIP-TiO_2/GR*

Because the most semiconductor oxides own amphoteric character, solution pH is one important factors causing the change of surface charge MIP-TiO_2/GR and the formation of hydroxyl radicals and influencing the degradation efficiency. The removal efficiency of BPA on MIP-TiO_2/GR is observed at the different pH values range from 3.0 to 10.0 and the results are shown in Fig. 9(a). The removal efficiency of BPA decreases obviously from 52.7% to 45.2% with increasing pH from 3.0 to 4.0, while increases remarkably from 45.2% to 55.3% with increasing pH from 4.0 to 5.0. When the pH is 5.0, the degradation rate of BPA reaches maximum. Then the removal efficiency of BPA changes little with increasing pH from 5.0 to 6.0, while decreases greatly with increasing pH from 6.0 to 8.0. Finally, the removal efficiency of BPA reaches minimum (44%) at pH to 10.

It is noticed that the removal efficiency of MIP-TiO_2/GR for BPA varies in the pH range studied and the variation is not so substantial by the research. The adsorption mode of BPA on MIP-TiO_2/GR surface and the formation of hydroxyl radicals should be considered as two main factors to explain the observed trend. The surface of MIP-TiO_2/GR is positively charged when the pH is low ($<pH_{pzc}$), and negatively charged when the pH is high ($>pH_{pzc}$). Meanwhile, it is found that the BPA molecule has two negative oxygen atoms at the hydroxyl groups and four negative carbon atoms at the phenolic group [36]. In addition, the pK_{a1} and pK_{a2} values of BPA are 9.6 and 10.2, and BPA tends to exist in its anionic form with further rise of solution pH [37]. Therefore, BPA can be attracted to the positively charged surface of MIP-TiO_2/GR at $pH \leq pH_{pzc}$, while repelled at $pH > pH_{pzc}$. We can see that the adsorption amount of MIP-TiO_2/GR for BPA in dark gradually reduce with the increase of pH value (Fig. 9(a)) and the result is consistent with the zeta potential and the above postulation. The adsorption of BPA over CN-TiO_2 has been found to exhibit similar trend in dark under different pH values by Wang and Lim [38]. Nevertheless, the concentration of hydroxyl radicals increases with the increase of pH [38], and increasing hydroxyl radicals can promote the degradation efficiency of BPA. Moreover, it's worth noting that the increase is limited since carbonate ions are generated as the byproduct during the oxidation process in the basic solution. The reaction of carbonate ions and hydroxyl radical can inhibit the formation and lower the oxidation potential of hydroxyl radicals [39–41]. Apparently, the variation trend of adsorption amount of BPA and the concentration of hydroxyl radicals are conflicting in the pH range studied. Hence, the removal efficiency for BPA varies and the variation is not so substantial. Meanwhile, the optimum pH on degradation of BPA exists and the optimum condition is the pH value from 5.0 to 6.0.

3.5.3. *Effects of initial BPA concentration on degradation of BPA on MIP-TiO_2/GR*

The removal efficiency of BPA on MIP-TiO_2/GR was investigated by changing the initial BPA concentration with a pH of 6.00, a catalyst concentration of 1.0 g/L and the degradation time of 180 min under visible light irradiation. The initial BPA concentration was adjusted to 4 mg/L, 8 mg/L, 16 mg/L, 24 mg/L and 32 mg/L, respectively. The result is shown in Fig. 9(b). We observe that the removal efficiency of BPA decreases with the increase of initial concentrations of BPA. The removal efficiency of BPA of MIP-TiO_2/GR decreases from 67.6% to 29.9% and the removal efficiency of BPA of NIP-TiO_2/GR decreases from 49.1% to 17.0% at the initial concentrations of BPA changing from 4 mg/L to 32 mg/L. When BPA initial concentration is 4 mg/L, the removal rate of BPA reaches maximum.

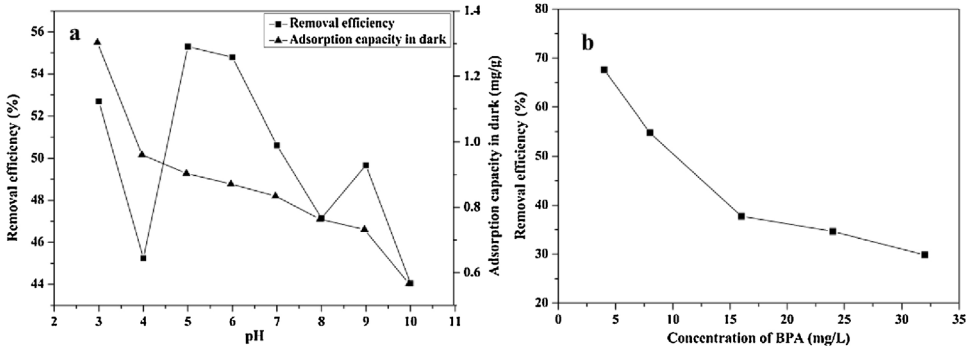

Fig. 9. Effect of initial pH (a) on removal efficiency of BPA and adsorption amount for bisphenol A in dark and effects of initial BPA concentration (b) on removal efficiency of BPA by MIP-TiO_2/GR.

The reason of this phenomenon may be that the active sites on the catalyst are blocked by the BPA molecule adsorbed on the catalyst surface with the increase of initial concentration of BPA [36]. Thereby, the amount of reactive hydroxyl free radicals as the main force of degradation of BPA decrease and the removal efficiency of BPA decreases. Additionally, the molar ratio of photocatalyst/BPA is lower for the higher BPA concentrated solution as a result of remaining the photocatalyst concentration unchanged at the different concentrations of BPA [42]. The more reactive hydroxyl free radicals produced by photocatalyst are favorable for the degradation of BPA.

3.6. Photocatalytic mechanism of MIP-TiO_2/GR photocatalyst

The photodegradation mechanism of BPA on MIP-TiO_2/GR photocatalyst can be described as follows. Firstly, the target molecules of BPA are adsorbed onto the MIP-TiO_2/GR surface. Then, the electron-hole pairs will be produced following the irradiation of MIP-TiO_2/GR photocatalyst with the visible light. The photogenerated electrons (e_{cb}^-) have strong reduction ability, and the photogenerated holes (h_{vb}^+) have strong oxidizing property. Therefore, the electron acceptors such as O_2 adsorbed on the surface of photocatalyst or dissolved in water can be reduced to superoxide radical anion ($^{\bullet}O_2^-$) by photogenerated electrons. Meanwhile, OH^- or H_2O can be oxidized to hydroxyl radicals ($^{\bullet}OH$) by the photogenerated holes [43,44]. The resulting $^{\bullet}OH$ react with BPA to carbon dioxide and water in the end.

$$\text{MIP-TiO}_2\text{/GR} + h\nu \rightarrow \text{MIP-TiO}_2\text{/GR}(e_{cb}^- + h_{vb}^+) \quad (6)$$

$$e_{cb}^- + O_2 \rightarrow {}^{\bullet}O_2^- \quad (7)$$

$$h_{vb}^+ + H_2O \rightarrow H^+ + {}^{\bullet}OH \quad (8)$$

$$h_{vb}^+ + OH^- \rightarrow {}^{\bullet}OH \quad (9)$$

$$^{\bullet}OH + \text{BPA} \rightarrow \text{degradation products} \quad (10)$$

4. Conclusion

Firstly, TiO_2/GR photocatalyst was synthesized according to a facile solvothermal synthesis method. After that, the surface molecular imprinting technique was used to modify the TiO_2/GR photocatalyst with BPA as the template molecule and OPDA as functional monomers so that MIP-TiO_2/GR photocatalyst was produced. MIP-TiO_2/GR photocatalyst exhibited fast dynamics, high adsorbing capacity and satisfactory selectivity by the affinity to the template molecules from the molecular imprinted cavities matched the structure of template molecules. Meanwhile, MIP-TiO_2/GR showed higher photocatalytic activity than NIP-TiO_2/GR attributing to the higher adsorption capacity, specific recognition ability for BPA and narrow band gap energy. So, MIP-TiO_2/GR photocatalyst exhibited a highly efficient photocatalytic degradation of bisphenol A under visible light irradiation in wastewater treatment. This work demonstrated that the surface molecular imprinting method was an effective approach to enhance the catalytic efficiency of the photocatalyst for target pollutant.

Acknowledgements

We would like to thank the Program for the Nation Natural Science Foundation of China (51378190, 51278176, 51408206, 51579098, 51521006), the National Program for Support of Top–Notch Young Professionals of China (2014), the Fundamental Research Funds for the Central Universities, the Program for New Century Excellent Talents in University (NCET-13-0186), the Program for Changjiang Scholars and Innovative Research Team in University (IRT-13R17), Scientific Research Fund of Hunan Provincial Education Department (No. 521293050) support of this study.

References

[1] W.L. Guo, W. Hu, J.M. Pan, H.C. Zhou, W. Guan, X. Wang, J.D. Dai, L.C. Xu, Selective adsorption and separation of BPA from aqueous solution using novel molecularly imprinted polymers based on kaolinite/Fe_3O_4 composites, Chem. Eng. J. 171 (2011) 603–611.
[2] Y.M. Ren, J. Yang, W.Q. Ma, J. Ma, J. Feng, X.L. Liu, The selective binding character of a molecular imprinted particle for bisphenol A from water, Water Res. 50 (2014) 90–100.
[3] C. Zhang, G.M. Zeng, D.L. Huang, C. Lai, C. Huang, N.J. Li, P. Xu, M. Cheng, Y.Y. Zhou, W.W. Tang, Combined removal of di(2-ethylhexyl) phthalate (DEHP) and Pb(ii) by using a cutinase loaded nanoporous gold-polyethyleneimine adsorbent, RSC Adv. 4 (2014) 55511–55518.
[4] C. Zhang, C. Lai, G.M. Zeng, D.L. Huang, L. Tang, C.P. Yang, Y.Y. Zhou, L. Qin, M. Cheng, Nanoporous Au-based chronocoulometric aptasensor for amplified detection of Pb^{2+} using DNAzyme modified with Au nanoparticles, Biosens. Bioelectron. 81 (2016) 61–67.
[5] K. Inumaru, M. Murashima, T. Kasahara, S. Yamanaka, Enhanced photocatalytic decomposition of 4-nonylphenol by surface-organografted TiO_2: a combination of molecular selective adsorption and photocatalysis, Appl. Catal. B: Environ. 52 (2004) 275–280.
[6] J.J. Tian, H.P. Gao, H.M. Deng, L. Sun, H. Kong, P.X. Yang, J.H. Chu, Structural, magnetic and optical properties of Ni-doped TiO_2 thin films deposited on silicon(100) substrates by sol-gel process, J. Alloys Compd. 581 (2013) 318–323.
[7] X. Bai, X.Y. Zhang, Z.L. Hua, W.Q. Ma, Z.Y. Dai, X. Huang, H.X. Gu, Uniformly distributed anatase TiO_2 nanoparticles on graphene: synthesis, characterization, and photocatalytic application, J. Alloys Compd. 599 (2014) 10–18.
[8] R. Leary, A. Westwood, Carbonaceous nanomaterials for the enhancement of TiO_2 photocatalysis, Carbon 49 (2011) 741–772.
[9] L. Zhao, M.D. Han, J.S. Lian, Photocatalytic activity of TiO_2 films with mixed anatase and rutile structures prepared by pulsed laser deposition, Thin Solid Films 516 (2008) 3394–3398.
[10] S. Buddee, S. Wongnawa, U. Sirimahachai, W. Puetpaibool, Recyclable UV and visible light photocatalytically active amorphous TiO_2 doped with M (III) ions (M = Cr and Fe), Mater. Chem. Phys. 126 (2011) 167–177.
[11] X.B. Luo, F. Deng, L.J. Min, S.L. Luo, B. Guo, G.S. Zeng, C. Au, Facile one-step synthesis of inorganic-framework molecularly imprinted TiO_2/WO_3

nanocomposite and its molecular recognitive photocatalytic degradation of target contaminant, Environ. Sci. Technol. 47 (2013) 7404–7412.
[12] J.J. Wang, Y.H. Jing, T. Ouyang, Q. Zhang, C.T. Chang, Photocatalytic reduction of CO_2 to energy products using Cu-TiO_2/ZSM-5 and Co-TiO_2/ZSM-5 under low energy irradiation, Catal. Commun. 59 (2015) 69–72.
[13] L. Samiolo, M. Valigi, D. Gazzoli, R. Amadelli, Photo-electro catalytic oxidation of aromatic alcohols on visible light-absorbing nitrogen-doped TiO_2, Electrochim. Acta 55 (2010) 7788–7795.
[14] J. Yang, J. Dai, J.T. Li, Synthesis, characterization and degradation of bisphenol A using Pr N co-doped TiO_2 with highly visible light activity, Appl. Surf. Sci. 257 (2011) 8965–8973.
[15] Y. Bessekhouad, N. Chaoui, M. Trzpit, N. Ghazzal, D. Robert, J. Weber, UV–vis versus visible degradation of Acid Orange II in a coupled CdS/TiO_2 semiconductors suspension, J. Photochem. Photobiol. A: Chem. 183 (2006) 218–224.
[16] K. Vinodgopal, P.V. Kamat, Enhanced rates of photocatalytic degradation of an azo dye using SnO_2/TiO_2 coupled semiconductor thin films, Environ. Sci. Technol. 29 (1995) 841–845.
[17] G. Marci, V. Augugliaro, M.J. Lopez-Munoz, C. Martin, L. Palmisano, V. Rives, M. Schiavello, R.J. Tilley, A.M. Venezia, Preparation characterization and photocatalytic activity of polycrystalline ZnO/TiO_2 systems. 2. Surface, bulk characterization, and 4-nitrophenol photodegradation in liquid-solid regime, J. Phys. Chem. B 105 (2001) 1033–1040.
[18] C. Liu, Y.J. Li, P. Xu, M. Li, M.X. Zeng, Controlled synthesis of ordered mesoporous TiO_2-supported on activated carbon and pore–pore synergistic photocatalytic performance, Mater. Chem. Phys. 149 (2015) 69–76.
[19] C. Langford, M. Izadifard, E. Radwan, G. Achari, Some observations on the development of superior photocatalytic systems for application to water purification by the adsorb and shuttle or the interphase charge transfer mechanisms, Molecules 19 (2014) 19557–19572.
[20] M. Ito, S. Fukahori, T. Fujiwara, Adsorptive removal and photocatalytic decomposition of sulfamethazine in secondary effluent using TiO_2-zeolite composites, Environ. Sci. Pollut. Res. 21 (2014) 834–842.
[21] K.R. Reddy, M. Hassan, V.G. Gomes, Hybrid nanostructures based on titanium dioxide for enhanced photocatalysis, Appl. Catal. A: Gen. 489 (2015) 1–16.
[22] A. Rey, D.H. Quinones, P.M. Álvarez, F.J. Beltrán, P.K. Plucinski, Simulated solar-light assisted photocatalytic ozonation of metoprolol over titania-coated magnetic activated carbon, Appl. Catal. B: Environ. 111 (2012) 246–253.
[23] X.F. Yang, J.L. Qin, Y. Li, R.X. Zhang, H. Tang, Graphene-spindle shaped TiO_2 mesocrystal composites: facile synthesis and enhanced visible light photocatalytic performance, J. Hazard. Mater. 261 (2013) 342–350.
[24] T.D. Nguyen-Phan, V.H. Pham, E.W. Shin, H.D. Pham, S. Kim, J.S. Chung, E.J. Kim, S.H. Hur, The role of graphene oxide content on the adsorption-enhanced photocatalysis of titanium dioxide/graphene oxide composites, Chem. Eng. J. 170 (2011) 226–232.
[25] C. Zhang, C. Lai, G.M. Zeng, D.L. Huang, C.P. Yang, Y. Wang, Y.Y. Zhou, M. Cheng, Efficacy of carbonaceous nanocomposites for sorbing ionizable antibiotic sulfamethazine from aqueous solution, Water Res. 95 (2016) 103–112.
[26] E. Lee, J.Y. Hong, H. Kang, J. Jang, Synthesis of TiO_2 nanorod-decorated graphene sheets and their highly efficient photocatalytic activities under visible-light irradiation, J. Hazard. Mater. 219 (2012) 13–18.
[27] Z.Q. Wang, X. Liu, W.Q. Li, H.Y. Wang, H.X. Li, Enhancing the photocatalytic degradation of salicylic acid by using molecular imprinted S-doped TiO_2 under simulated solar light, Ceram. Int. 40 (2014) 8863–8867.
[28] H.Q. Tang, L.H. Zhu, C. Yu, X.T. Shen, Selective photocatalysis mediated by magnetic molecularly imprinted polymers, Sep. Purif. Technol. 95 (2012) 165–171.
[29] X.T. Shen, L.H. Zhu, G.X. Liu, H.W. Yu, H.Q. Tang, Enhanced photocatalytic degradation and selective removal of nitrophenols by using surface molecular imprinted titania, Environ. Sci. Technol. 42 (2008) 1687–1692.
[30] F.F. Duan, C.Q. Chen, L. Chen, Y.J. Sun, Y.W. Wang, Y.Z. Yang, X.G. Liu, Y. Qin, Preparation and evaluation of water-compatible surface molecularly imprinted polymers for selective adsorption of bisphenol A from aqueous solution, Ind. Eng. Chem. Res. 53 (2014) 14291–14300.
[31] X.T. Shen, L.H. Zhu, J. Li, H.Q. Tang, Synthesis of molecular imprinted polymer coated photocatalysts with high selectivity, Chem. Commun. (2007) 1163–1165.
[32] D.C. Marcano, D.V. Kosynkin, J.M. Berlin, A. Sinitskii, Z. Sun, A. Slesarev, L.B. Alemany, W. Lu, J.M. Tour, Improved synthesis of graphene oxide, ACS Nano 4 (2010) 4806–4814.
[33] F. Deng, Y.X. Li, X.B. Luo, L.X. Yang, X.M. Tu, Preparation of conductive polypyrrole/TiO_2 nanocomposite via surface molecular imprinting technique and its photocatalytic activity under simulated solar light irradiation, Coll. Surf. A 395 (2012) 183–189.
[34] F. Deng, Y. Liu, X.B. Luo, S.L. Wu, S.L. Luo, C. Au, R.X. Qi, Sol-hydrothermal synthesis of inorganic-framework molecularly imprinted TiO_2/SiO_2 nanocomposite and its preferential photocatalytic degradation towards target contaminant, J. Hazard. Mater. 278 (2014) 108–115.
[35] H.L. Wang, D.Y. Zhao, W.F. Jiang, Synthesis and photocatalytic activity of poly-o-phenylenediamine (PoPD)/TiO_2 composite under VIS-light irradiation, Synth. Met. 162 (2012) 296–302.
[36] R.C. Wang, D.J. Ren, S.Q. Xia, Y.L. Zhang, J.F. Zhao, Photocatalytic degradation of bisphenol A (BPA) using immobilized TiO_2 and UV illumination in a horizontal circulating bed photocatalytic reactor (HCBPR), J. Hazard. Mater. 169 (2009) 926–932.
[37] P.G. Kosky, J.M. Silva, E.A. Guggenheim, The aqueous phase in the interfacial synthesis of polycarbonates. Part 1. Ionic equilibria and experimental solubilities in the BPA-sodium hydroxide-water system, Ind. Eng. Chem. Res. 30 (1991) 462–467.
[38] X.P. Wang, T.T. Lim, Solvothermal synthesis of C-N codoped TiO_2 and photocatalytic evaluation for bisphenol A degradation using a visible-light irradiated LED photoreactor, Appl. Catal. B: Environ. 100 (2010) 355–364.
[39] A.A. Joshi, B.R. Locke, P. Arce, W. Finney, Formation of hydroxyl radicals, hydrogen peroxide and aqueous electrons by pulsed streamer corona discharge in aqueous solution, J. Hazard. Mater. 41 (1995) 3–30.
[40] S. Dalhatou, C. Pétrier, S. Laminsi, S. Baup, Sonochemical removal of naphthol blue black azo dye: influence of parameters and effect of mineral ions, Int. J. Environ. Sci. Technol. 12 (2015) 35–44.
[41] C.F. Chang, C.Y. Man, Titania-coated magnetic composites as photocatalysts for phthalate photodegradation, Ind. Eng. Chem. Res. 50 (2011) 11620–11627.
[42] Y. Ahmed, Z. Yaakob, P. Akhtar, Degradation and mineralization of methylene blue using a heterogeneous photo-Fenton catalyst under visible and solar light irradiation, Catal. Sci. Technol. 6 (2016) 1222–1232.
[43] C.J. Zhang, H. Chen, M.J. Ma, Z.P. Yang, Facile synthesis of magnetically molecular recognitive photocatalytic degradation of target contaminant, J. Mol. Catal. A: Chem. 402 (2015) 10–16.
[44] Z.P. Yang, J.L. Yan, C.J. Zhang, S.Q. Luo, Enhanced removal of bilirubin on molecularly imprinted titania film, Colloids Surf. B: Biointerfaces 87 (2011) 187–191.